EUROPEAN ORGANIZATION FOR NUCLEAR RESEARCH

EB/afm

CERN/PS/85-45 (AA)

A MICROWAVE CERENKOV PICK-UP FOR STOCHASTIC COOLING

E. Brambilla
Technical Student, INFN, Sezione di Napoli, Italy

Geneva, Switzerland
June, 1985

CONTENTS

INTRODUCTION

In this report a wide-band pick-up for very high frequencies is described, in which the essential part is a dielectrically loaded wave guide (Fig. 1).

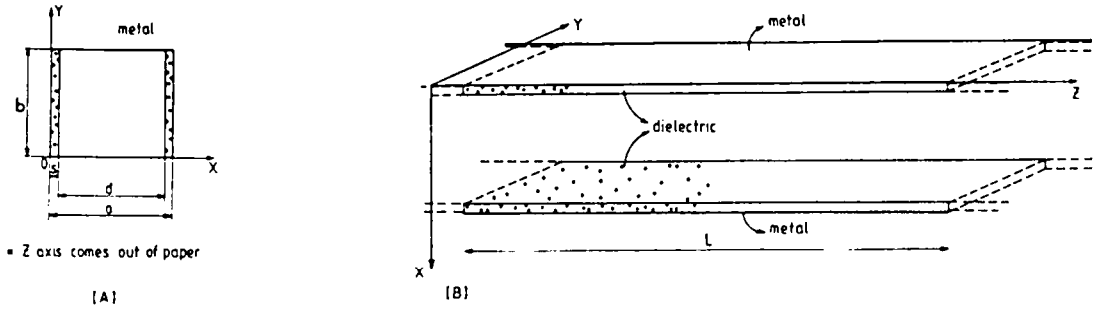

A) Cross section view of the pick-up.
a = total wave guide width,
b = total wave guide height,
s = dielectric slab thickness,
d = a-2s = distance between slabs.

B) Longitudinal view.
(Cut of the wave guide side metal walls).
L = length of the loaded wave guide.

Figure 1

The dielectric constant of the media filling the wave guide is a step function defined by:

$$\epsilon(x) = \begin{cases} \epsilon_r \epsilon_0 & 0 < x < s \; ; \quad s + d < x < a \\ \epsilon_0 & s < x < s + d \end{cases}$$

The main feature which makes this pick-up different from those usually employed is the continuous dielectric structure which is the support for the propagating signal. The simplicity of the structure makes the device eminently suitable for use in stochastic cooling systems either as pick-ups or kickers.

The physical effect underlying the power collection is the Cerenkov effect. It is briefly summarized in Section 1.

The approach used is to compute the beam-excited electromagnetic field through an expansion of this field over the normal modes of the dielectric-loaded wave guide. Coefficients of the expansion and power carried by the field are computed in Section 2. A definition for the sensitivity is also given in Section 2.

Equations obtained in Section 2 are employed to optimize the pick-up performance (Section 3) and lead to the design described in Section 4.

Parameters suitable for a pick-up which detects longitudinal beam structure in the Antiproton Accumulator are listed in Section 5.

This report summarizes the work carried out by the author on a technical studentship in the AA Group of the PS Division: it is part of a more extensive programme of research carried out by a CERN-Naples University collaboration[1].

1. THE CERENKOV EFFECT IN THE MICROWAVE REGION

The Cerenkov effect has been extensively studied in the literature[2,3,4]. The use of Cerenkov radiation for generating microwaves was proposed by Ginzburg in 1947. In the following years many attempts were made to build high-power generators for microwaves employing the Cerenkov effect[5,6,7,8].

Cerenkov radiation also appears to be suitable for detecting longitudinal beam structure when the beam is allowed to pass through a dielectrically loaded wave guide.

To understand how microwave power is produced when Cerenkov radiation occurs in a wave guide, one must recall the main features of the Cerenkov effect.

When a charged particle moves through an infinite dielectric medium, constructive interference can occur from the wave fronts produced by the particle along its way (Fig. 2), only if the following conditions are satisfied:

$$\beta_p n > 1 \; ; \qquad (v_\varphi)_z = v_p \; ,$$

where v_p = particle velocity,
v_φ = wave phase velocity,
β_p = v_p/c,
n = refractive index of the dielectric medium,
$(v_\varphi)_z$ = projection of wave phase velocity on the axis of particle motion.

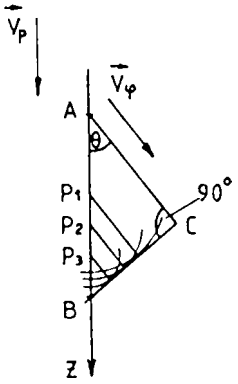

Figure 2
Huyghens construction to illustrate coherence of Cerenkov radiation.

Under these conditions Cerenkov radiation is observed propagating over a cone whose axis lies on the particle trajectory, and whose semi-aperture is $\theta = \arccos(1/\beta_p n)$.

Cerenkov radiation obviously depends on v_p and $n(\omega)$, where ω is the frequency of the radiation.

The picture changes if the charged particle moves in a finite structure, for instance in a loaded wave guide, such as that sketched in Fig. 3.

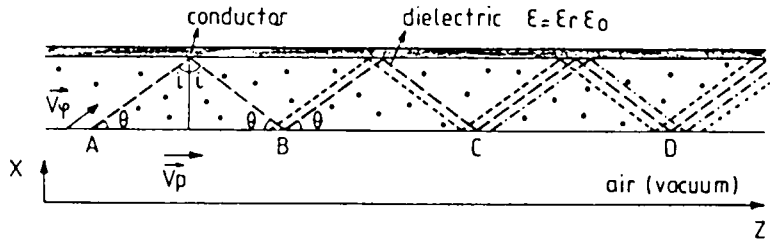

Figure 3 - Simplified view for capability to enhance Cerenkov power by a dielectrically loaded wave guide.

Reflections from the outer surface of the wave guide and from the air-dielectric interface must be taken into account.

Referring to Fig. 3, radiation produced at z = A at the Cerenkov angle $\theta = \arccos(1/\beta_p n)$ is reflected by the wave guide's outer conductor and is generally reflected again at air-dielectric interface with the incidence angle θ.

The condition for total internal reflection from the air-dielectric surface can be expressed in term of the field wave number k_0.

If

$$k_x^2 + k_y^2 + k_z^2 = k_0^2 \quad \text{in air,}$$

and

$$(k_x^d)^2 + k_y^2 + k_z^2 = \sqrt{\epsilon_r}\, k_0^2 \quad \text{in dielectric,}$$

hence

$$k_x^2 = (1 - \epsilon_r)k_0^2 + (k_x^d)^2.$$

Now

$$(k_x^d)^2 = \sqrt{\epsilon_r}\, k_0 \sin\theta \; ; \qquad \text{and } k_x^2 = (1 - \epsilon_r \cos^2\theta)k_0^2. \tag{1.1}$$

Total internal reflection (as in Fig. 3) means no propagation in the air, or k_x imaginary. This occurs if in (1.1):

$$\cos\theta > \frac{1}{\sqrt{\epsilon_r}} = \frac{1}{n} \; . \tag{1.2}$$

Cerenkov radiation occurs at the angle θ given by $\cos\theta = 1/\beta_p n$, so (1.2) is fulfilled by Cerenkov radiation ($\beta_p < 1$), which remains trapped in the slab of dielectric.

A new wave produced at z = B by the passage of the particle adds to the reflected wave from A if $(v_\varphi)_z = v_p$. Power in the dielectric obviously increases with slab length.

It is worth noting that most of the published literature generally employs cylindrically loaded wave guides, which fit the beam (or particle) geometry and simplifies the analysis.

Solutions for Cerenkov radiation by a charge passing along the axis of a rectangular loaded wave guide were not found in the literature.

2. *FIELDS AND NORMAL MODES IN RECTANGULAR DIELECTRIC LOADED WAVE GUIDES*

We look for the exact analytical expression of the electromagnetic field generated by a bunched beam moving along the z-direction (on the axis) into the empty (air or vacuum) region of the loaded wave guide (Fig. 1).

To this end we perform an expansion of the transverse components of the field over the normal modes of the wave guide.

2.1 Beam Model

In order to simplify the analytical treatment a point configuration is assumed for the transverse dimensions of the beam, described by the $\delta(x - a/2)\delta(y - b/2)$ function.

A single frequency of the Fourier spectrum is considered, expressing the (z, t) dependence through the factor $e^{j(\omega t - k_p z)}$, where $k_p = \omega/v_p$ is the beam propagation constant along z, with $v_p = c\beta_p$ the beam velocity (obviously c = free empty space light velocity) The expression given below is the Fourier transform of current into the frequency ω and z-wave number domains.

$$\vec{I}(x, y, \gamma, \omega) = I_0 \, \hat{z} \, \delta(x - a/2)\delta(y - b/2) e^{j\omega t} \int_{-\infty}^{\infty} e^{-jk_p z} \; e^{j\gamma z} \, dz \qquad (2.1)$$

where γ represents the generic z-wave number in the space-like frequency domain and I_0 is the d.c. beam current. The integral on the right of (2.1) converges if the finite length of the dielectric slab is taken into account, which is the same as assuming the model of a finite length L of current passing along an infinite slab of dielectric.

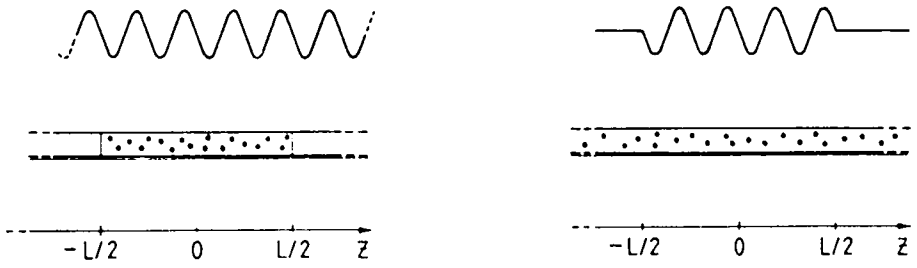

a) Real situation.

The finite length pick-up sees an infinite current.

b) The model.

An infinite dielectric slab, but a "square" wave function current.

Figure 4

In Fig. 4b the signal of a fixed z-space frequency (k_p) of Fig. 4a is multiplied by a "square" wave function of length L. This product can be decomposed into a Fourier spectrum. γ is any harmonic of the "square" wave. The factor $2 \cdot \sin\{(\gamma - k_p)L/2\}/(\gamma - k_p)$ is the weight of each Fourier harmonic to reproduce the original signal over the finite length L.

Hence the current transform is:

$$I(x, y, \gamma, \omega) = 2I_0 \, \delta(x - a/2)\delta(y - b/2) \, \frac{\sin\{(\gamma - k_p)L/2\}}{\gamma - k_p} \cdot e^{j\omega t} \; . \qquad (2.2)$$

2.2 Fields

We write $\vec{\mathcal{E}}$ and $\vec{H}$ in the ω-frequency and z-space frequency domains:

$$\vec{\mathcal{E}}(\vec{r}, t) = 1/(2\pi)^2 \int_{-\infty}^{\infty} d\omega \, e^{j\omega t} \int_{-\infty}^{\infty} e^{-j\gamma t} \, d\gamma \, \vec{E}(\underline{t}, \gamma, \omega) \; ; \quad \text{electric field} \qquad (2.3a)$$

$$\vec{H}(\vec{r},\ t) = 1/(2\pi)^2 \int_{-\infty}^{\infty} d\omega\ e^{j\omega t} \int_{-\infty}^{\infty} e^{-j\gamma t}\, d\gamma\ \vec{E}(\underline{t},\ \gamma,\ \omega)\ ;\quad \text{magnetic field} \tag{2.3b}$$

and solve Maxwell's equations for the transforms of $\vec{\mathcal{E}}$ and $\vec{H}$, namely $\vec{E}(\underline{t},\ \gamma,\ \omega)$ and $\vec{H}(\underline{t},\ \gamma,\ \omega)$, where $\underline{t}$ represents a unitary vector in the transverse plane of the wave guide.

Transverse components of $\vec{E}$ and $\vec{H}$ can be expanded in term of eigenvectors of the wave guide we are treating, employing the normal mode functions $\underline{e}_{mn}(\underline{t})$, $\underline{h}_{mn}(\underline{t})$ which are computed in Appendix 1. It is easily understood from the Appendix that indices refer to the order of the k_x and k_y wave numbers, respectively, as is usual for the finite structure eigenvectors. From here onwards, for the sake of brevity, we choose to use one index only for the eigenvectors.

$$\underline{E}_t(\underline{t}) = \sum_m c_m\ \underline{e}_m(\underline{t}) \tag{2.4a}$$

$$\underline{H}_t(\underline{t}) = \sum_m d_m\ \underline{h}_m(\underline{t}) \quad . \tag{2.4b}$$

Separating between transverse and longitudinal components of fields and sources, and indicating them with a "t" or "z" subscript, respectively, we get Maxwell's equations valid in each continuous region of the wave guide:

$$j\gamma \underline{E}_t = j\omega\mu_0 \left\{ I + \frac{1}{k^2(x)}\, \nabla_t \nabla_t \right\} \cdot (\underline{H}_t \cdot \hat{z}) + (\vec{I}_{mt})_{eq} \cdot \hat{z} \tag{2.5a}$$

$$j\gamma \underline{H}_t = j\omega\varepsilon(x) \left\{ I + \frac{1}{k^2(x)}\, \nabla_t \nabla_t \right\} \cdot (\hat{z} \cdot \underline{E}_t) + \hat{z} \cdot (I_{et})_{eq} \tag{2.5b}$$

where $k^2(x) = \omega^2 \varepsilon(x) \mu_0$. The magnetic permeabilities of the media are assumed to be constant and equal to free space permeability, μ_0,

$\varepsilon(x)$ = absolute dielectric constant of the medium wherein the above equations obtain.

and

$$(\vec{I}_{mt})_{eq} = \frac{\hat{z} \cdot \nabla_t I_{ez}}{j\omega\varepsilon(x)} + \vec{I}_{mt} \tag{2.6a}$$

$$(\vec{I}_{et})_{eq} = \frac{\nabla_t I_{mz} \cdot \hat{z}}{j\omega\mu_0} + \vec{I}_{et} \quad . \tag{2.6b}$$

A pair of equations like (2.5) but with no current terms hold for eigenvectors $\underline{e}$, $\underline{h}$ of each normal mode.

$$j\gamma_m \underline{e}_m = j\omega\mu_0 \left\{ I + \frac{1}{k^2(x)}\, \nabla_t \nabla_t \right\} \cdot (\underline{h}_m \cdot \hat{z}) \tag{2.7a}$$

$$j\gamma_m \underline{h}_m = j\omega\varepsilon(x) \left\{ I + \frac{1}{k^2(x)}\, \nabla_t \nabla_t \right\} \cdot (\hat{z} \cdot \underline{e}_m) \tag{2.7b}$$

where γ_m is the propagation wave number of the m-mode, as appearing in Appendix 1, (A.4). Putting (2.4) into (2.5), taking into account the orthogonal properties (A.13) of the eigenvectors and the equations (2.7), we can get the analytical expression for the coefficients c_m, d_m of (2.4). Namely,

$$j\gamma c_m = d_m j\gamma_m + \frac{1}{j\omega\varepsilon(x)} \int_0^b dy \int_0^a dx(\nabla_t I_{ez} \cdot \underline{h}_m^*) \cdot \hat{z} \tag{2.8a}$$

$$d_m = \frac{\gamma_m}{\gamma} c_m \quad . \tag{2.8b}$$

The symbol "*" serves to indicate the operation of complex conjugation.

This equality holds (see Appendix 3):

$$\int_0^b dy \int_0^a dx(\nabla_t I_{ez} \cdot h_m^*) \cdot \hat{z} = j\omega\varepsilon(x) \int_0^b dy \int_0^a dx(I_{ez} e_{zm}^*) \tag{2.9}$$

where e_{zm} is the z-component of the eigenvector of normal mode $\underline{e}_m$.

Expressing I_{ez} through (2.2) and performing the integral on the right of (2.9) we get:

$$c_m = 2I_0 \, C_m(\gamma) \, e_{zm}^* \left(\frac{a}{2} , \frac{b}{2}\right) \tag{2.10a}$$

$$d_m = 2I_0 \, D_m(\gamma) \, e_{zm}^* \left(\frac{a}{2} , \frac{b}{2}\right) \tag{2.10b}$$

where

$$C_m(\gamma) = \frac{-j\gamma}{(\gamma^2 - \gamma_m^2)} \quad \frac{\sin\{(\gamma - k_p)L/2\}}{\gamma - k_p} \tag{2.11a}$$

$$D_m(\gamma) = \frac{-j\gamma_m}{(\gamma^2 - \gamma_m^2)} \quad \frac{\sin\{(\gamma - k_p)L/2\}}{\gamma - k_p} \tag{2.11b}$$

and $e_z^*(a/2, b/2)$ means that the e_z-function must be evaluated at the beam, on the axis of the wave guide.

To get reasonable values of dielectric slab thickness, Longitudinal-Section Magnetic (LSM) modes must be excited by the beam (see next section). Hence in expression (2.4) we restrict ourselves to LSM eigenvectors only. Moreover, we expect to keep below the cut-off frequency of the higher order LSM modes, so that only the first LSM mode is excited.

If this condition is satisfied the summation in (2.4) reduces to:

$$\underline{E}_t(\underline{t}) = c_1 \, \underline{e}_1(\underline{t}) \tag{2.12a}$$

$$\underline{H}_t(\underline{t}) = d_1 \, \underline{h}_1(\underline{t}) \tag{2.12b}$$

Fields expressed by (2.12) are maintained under the integrals in (2.3). Integration over γ of fields expressed by (2.12) affects only factors $C_1(\gamma)$ and $D_1(\gamma)$ for $\underline{E}_t$ and $\underline{H}_t$, respectively. Allowing for poles appearing in (2.11), we perform the integrals over γ and obtain:

$$\underline{E}_t(\vec{r},\ \omega) = 2I_0\ F_1(\gamma_1,\ z)\ e^*_{z_1}\left(\frac{a}{2}\ ,\ \frac{b}{2}\right)\underline{e}^{LSM}_{t_1}(x,\ y)e^{j\omega t} \tag{2.13a}$$

$$\underline{H}_t(\vec{r},\ \omega) = 2I_0\ K_1(\gamma_1.\ z)\ e^*_{z_1}\left(\frac{a}{2}\ ,\ \frac{b}{2}\right)\underline{h}^{LSM}_{t_1}(x,\ y)e^{j\omega t} \tag{2.13b}$$

where, for the generic m-mode:

$$F_m(\gamma_m,\ z) = \frac{1}{2}\left[e^{-j(\gamma_m+k_p)L/2}\ e^{j(\gamma_m-k_p)z/2}\ \frac{\sin\{(k_p+\gamma_m)(L/2-z)/2\}}{\gamma_m+k_p} + \right.$$
$$\left. -e^{j(k_p-\gamma_m)L/2}\ e^{-j(k_p+\gamma_m)z/2}\ \frac{\sin\{(k_p-\gamma_m)(L/2+z)/2\}}{k_p-\gamma_m}\right] \tag{2.14a}$$

$$K_m(\gamma_m,\ z) = \frac{1}{2}\left[-e^{-j(\gamma_m+k_p)L/2}\ e^{j(\gamma_m-k_p)z/2}\ \frac{\sin\{(k_p+\gamma_m)(L/2-z)/2\}}{k_p-\gamma_m} + \right.$$
$$\left. -e^{j(k_p-\gamma_m)L/2}\ e^{-j(k_p+\gamma_m)z/2}\ \frac{\sin\{(k_p-\gamma_m)(L/2+z)/2\}}{k_p-\gamma_{mn}}\right] \tag{2.14b}$$

The expressions for the fields are valid in the range $z \in [-L/2,\ L/2]$ (coordinates refer to Fig. 4).

Manipulation of (2.14) yields fields which can be written in the form, where sine x = sinx/x:

$$\underline{E}_t(\vec{r},\ \omega) = \gamma_1\ q\ \varepsilon_r\ A_0\ \frac{\cos ps}{\sinh qd/2}\ I_0\left\{-j\ e^{-j(\gamma_1+k_p)L/2}\ e^{j(\gamma_1-k_p)z/2}\ \frac{(L/2-z)}{2}\ \cdot\right.$$
$$\cdot\ \text{sine}\left[\frac{\gamma_1+k_p}{2}\left(\frac{L}{2}-z\right)\right] + j\ e^{j(k_p-\gamma_1)L/2}\ e^{-j(k_p+\gamma_1)z/2}\ \frac{(L/2+z)}{2}\ \cdot$$
$$\left.\cdot\ \text{sine}\left[\frac{k_p-\gamma_1}{2}\left(\frac{L}{2}+z\right)\right]\right\}\underline{e}^{LSM}_1(x,\ y)e^{j\omega t} \tag{2.15a}$$

$$\underline{H}_t(\vec{r},\ \omega) = \gamma_1\ q\ \varepsilon_r\ A_0\ \frac{\cos ps}{\sinh qd/2}\ I_0\left\{j\ e^{-j(\gamma_1+k_p)L/2}\ e^{j(\gamma_1-k_p)z/2}\ \frac{(L/2-z)}{2}\ \cdot\right.$$
$$\cdot\ \text{sine}\left[\frac{\gamma_1+k_p}{2}\left(\frac{L}{2}-z\right)\right] + j\ e^{j(k_p-\gamma_1)L/2}\ e^{-j(k_p+\gamma_1)z/2}$$
$$\left.\cdot\ \frac{(L/2+z)}{2}\ \text{sine}\left[\frac{k_p-\gamma_1}{2}\left(\frac{L}{2}+z\right)\right]\right\}\underline{e}^{LSM}_1(x,\ y)e^{j\omega t}\ , \tag{2.15b}$$

where q and p are the lowest order roots of the LSM dispersion equation and A_o is the normalization factor for odd LSM eigenfunctions, as shown in Appendix 1, (A.14).

The "sine" function requires the synchronism between the normal mode in the wave guide and the beam, to get the maximum response of the pick-up. This condition can be written $\gamma_1 = \pm k_p$, where the sign is referred to a beam propagating respectively along positive (as in our case) or negative z-axis.

By the choice $\gamma_1 = k_p$ we can ignore the wave propagating along the negative z-axis, because of the small amplitude of sine $\{(k_p + \gamma_1)(L/2 - z)/2\}$, and write the synchronous field as:

$$\underline{E}_t(\vec{r}, \omega) = jk_p q\, \varepsilon r\, A_o \frac{\cos ps}{\sinh qd/2} I_0 \frac{1}{2}\left(\frac{L}{2} + z\right) \underline{e}_1^{LSM}(x, y)\, e^{j(\omega t - k_p z)} \qquad (2.16a)$$

$$\underline{H}_t(\vec{r}, \omega) = jk_p q\, \varepsilon r\, A_o \frac{\cos ps}{\sinh qd/2} I_0 \frac{1}{2}\left(\frac{L}{2} + z\right) \underline{h}_1^{LSM}(x, y)\, e^{j(\omega t - k_p z)} \qquad (2.16b)$$

2.3 Cerenkov Comparison

The results of this approach are in agreement with the expectations from the classical Cerenkov effect.

As is shown in expression (2.16) a bunched beam passing near a dielectric surface in a wave guide generates waves which propagate in the direction of motion of the beam. A discrete spectrum is selected at those frequencies for which synchronism between the beam and wave velocities occurs.

Expression (2.16) shows that the longer the dielectric slab, the greater is the quantity of power generated, in agreement with what was stated in Section 1.

2.4 Power Flux

When the synchronous condition is satisfied, expression (2.16) enables us to compute the power flowing along $\hat{z}$ across the wave guide cross-section at $z = L/2$, due to the passage of the beam.

At a fixed harmonic, power flowing in the total cross sectional area is:

$$P_z^{(\omega)} = \frac{1}{2} \mathrm{Re} \int_0^b dy \int_0^a dx (\underline{E}_t \cdot \underline{H}_t^*) \cdot \hat{z} \quad . \qquad (2.17)$$

Similarly the power flowing in the dielectric slabs or alternatively in the empty region, can be computed.

The expressions for the power flowing in the <u>total</u> cross sectional area of the guide and in the two <u>dielectric</u> slabs are:

$$[P_z^{(\omega)}(z = L/2)]_{total} = \frac{1}{2}\left\{k_p\, q\, \varepsilon_r\, A_o \frac{\cos ps}{\sinh qd/2} I_0 \frac{L}{2}\right\}^2 \qquad (2.18)$$

$$[P_z^{(\omega)}(z = L/2)]_{diel} = \frac{1}{2}\left\{k_p\, q\, \varepsilon_r\, A_0\, \frac{\cos ps}{\sinh qd/2}\, I_0\, \frac{L}{2}\right\}^2 \frac{1}{G_0}\,\frac{1}{2}\left(s + \frac{\sin 2ps}{2ps}\right) \qquad (2.19)$$

where G_0 is expressed by (A.15b) of Appendix 1.

The ratio between power flowing in the dielectric medium and total power (used for pick-up design and optimization) is given by:

$$\frac{P_z^{\omega}(diel)}{P_z^{\omega}(tot)} = \frac{s(1 + \sin 2ps/2ps)}{2G_0} \qquad (2.20)$$

When the synchronous condition is not completely fulfilled, as can happen if the beam fre-frequencies change, the time-average power flowing across the wave guide section at the end z = L/2, computed from (2.17), is:

$$P_z^{(\omega)}(z = L/2) = \frac{1}{2}\left[\gamma_m\, q_m\, \varepsilon_r\, A_0\, \frac{\cosh_m s}{\sinh q_m d/2}\right]^2 I_0^2 \left(\frac{L}{2}\right)^2 * \left[\text{sine}\ (k_p - \gamma_m)L/2\right]^2 . \qquad (2.21)$$

To emphasize that all three wave numbers change when synchronism does not hold any more, we indicate them with the generic subscripts m.

2.5 Sensitivity

The sensitivity S of a pick-up may be defined as:

$$S = \frac{V_0}{I_0} \qquad (2.22)$$

where V_0 is the output voltage picked up on a probe antenna, placed suitably near to the dielectric, with characteristic impedance Z_A, and I_0 is the d.c. beam current.

It is easy to write (2.22) in terms of the total power carried by the LSM1 mode. On the antenna

$$V_0 = I_A\, Z_A \qquad (2.23)$$

where I_A is the current flowing in the antenna; the output power can be written:

$$P_0 = V_0\, I_A \qquad (2.24)$$

From (2.23):

$$I_A = \frac{V_0}{Z_A}$$

and from (2.24)

$$V_0 = \frac{P_0}{I_A} \quad ,$$

so we can write:

$$\frac{V_0}{I_0} = \frac{P_0}{I_0}\frac{Z_A}{V_0} \quad \text{or} \quad \frac{V_0^2}{I_0^2} = \frac{P_0}{I_0^2} Z_A \tag{2.25}$$

Thus expression (2.22) becomes:

$$S^2 = \frac{P_0}{I_0^2} Z_A \quad . \tag{2.26}$$

Making the assumption that the whole output power is carried by the LSM1 MODE (no higher order modes excited) and flowing entirely in the dielectric (as will be clarified later), P_0 can be written like (2.18), or (2.21) if the chosen mode is not synchronous, and the analytical expression for S can be obtained.

3. *PICK-UP OPTIMIZATION*

Optimization of the pick-up means choosing the parameters involved in the previous theory, so that the pick-up can give the best response to the beam passage. The pick-up must have two important properties:

1. a large value of sensitivity: from the definition (2.26) this means that the beam must excite the largest possible quantity of total power in the wave guide.
2. a very large value of power flowing in the dielectric slabs compared with the total power in the wave guide, since the former becomes the signal to be detected.

It is useful to describe in a few words the physical meaning of the two points above.

The first property means the beam needs to be strongly coupled to the field distribution of the first mode in the wave guide. This can be seen from (2.10) where, through (2.9), e_z^* estimated at the beam appears.

The second property asks that the total power distributes itself mainly in the dielectric rather than in air, this means decreasing the amplitude of e.m. field in the space between the slabs.

As these two properties are somewhat contradictory to each other, it is necessary to study them apart for the optimization process.

3.1 Optimization of Sensitivity

The key-relations for optimization of sensitivity are:

a) the expression (2.26) for the sensitivity,
b) the synchronism condition,
c) the dispersion equations (A.10a) or (A.11b),
d) the wave number relations (A.9b), (A.9c).

The parity of modes has been selected so that, according to (2.10a, 2.10b), the z-component of the electric field of the excited mode is not zero at the beam. In this treatment, assuming a beam passing along the centre of the wave guide, we select those modes which give a symmetric e_z- distribution around x = a/2 in the air region, namely odd LSM modes and even LSE modes (following the nomenclature in Appendix 1).

Like wise, from the symmetry, only LSM modes with odd "n" index or LSE modes with even "n" can be excited by the beam. Obviously a pick-up sensitive to the transverse displacement of the beam position could be realized by employing the modes with anti-symmetrical distribution of e_z[1].

The dispersion relation of LSE modes (A.10a) shows a cut-off frequency, because it has no roots until the argument "ps" is at least $\pi/2$. LSM modes have no cut off-frequency and may exist for the smallest of slab thicknesses. Hence they are most suitable for our needs.

For this reason we design the pick-up for operation in the first LSM mode (disp. equation A.11b). As was said in section 2, the main property to be "matched" for maximum response of the device is mode-beam synchronism, namely:

$$\gamma_1 = kp \ . \tag{3.1}$$

Using (3.1) in (A.9) we get:

$$p^2 = \frac{k_0^2}{\beta_p^2} (\epsilon_r \beta_p^2 - 1) - \left(\frac{\pi}{b}\right)^2 \tag{3.2a}$$

$$q^2 = \frac{k_0^2}{\beta_p^2} (1 - \beta_p^2) + \left(\frac{\pi}{b}\right)^2 \ , \tag{3.2b}$$

while (A.9c) is still valid.

Converting to dimensionless parameters, namely wave number normalized to k_0 (the unbounded empty space wave number) and length multiplied by $k_0 (= 2\pi/\lambda_0)$, let us optimize the pick-up while ignoring for the moment the working frequency.

The expression for sensitivity in terms of dimensionless parameters, from (2.26), is given below: (3.3)

$$S = \sqrt{Z_A} \cdot k_0 \cdot \frac{L}{2} \sqrt{\frac{1}{2} \left\{ \bar{\gamma}_m \frac{\bar{q}_m^2}{(1 + \bar{q}_m^2)} \epsilon_r \frac{\cos^2 \bar{p}_m \bar{s}}{\sinh^2 \bar{q}_m \bar{d}/2} Z_0 \frac{1}{\bar{b}} \frac{1}{\bar{G}_o} \right\}} \cdot \operatorname{sine}\left[k_0 \left(\frac{1}{\beta_p} - \bar{\gamma}_m \right) L/2 \right]$$

where Z_0 (the unbounded empty space impedance) $= \sqrt{\mu_0/\epsilon_0}$; the bars indicate normalized quantities, and wave numbers p_m, q_m, γ_m refer to a generic LSM mode. When synchronism is satisfied, (3.3) reduces:

$$S = \sqrt{Z_A} \cdot k_0 \cdot \frac{L}{2} \sqrt{\frac{1}{2} \left\{ \frac{1}{\beta_p} \frac{\bar{q}^2}{(1 + \bar{q}^2)} \epsilon_r \frac{\cos^2 \bar{p}\, \bar{s}}{\sinh^2 \bar{q}\bar{d}/2} Z_0 \frac{1}{\bar{b}} \frac{1}{\bar{G}_0} \right\}} \tag{3.4}$$

where $\bar{q}$, $\bar{p}$ are the wave numbers corresponding to the case when $\gamma_m = kp$. Before optimizing we need to fix a few parameters: for instance the minimum distance between slabs (d), which is related to maximum beam horizontal size, and a convenient value of dielectric

constant ($\varepsilon_r\varepsilon_0$); β_p is known. In order to choose the optimum value of slab thickness (s), synchronism must be imposed and the behaviour of sensitivity (3.4) versus normalized s must be investigated.

This can be done through a computer program: the plot of Fig. 9 refers to the case studied for the CERN antiproton accumulator AA; $\bar{b}$ depends on the value of $\bar{s}$, through (3.2b), as do $\bar{p}$ and $\bar{q}$.

When $\bar{s}$ is chosen, in order to get the maximum sensitivity, we can fix the working frequency and get the real dimensions for lengths and wave numbers. Once the pick-up cross-section is fixed, the bandwidth for a fixed slab length can be estimated through expression (3.3). p, q, γ_1 change with frequency: they are solutions of the system of equations (A.11b), (A.9b) and (A.9c). Figure 11 shows sensitivity versus frequency for the case of the AA pick-up.

It can happen that the maximum sensitivity does not correspond exactly to the beam-mode synchronization frequency: this happens because the synchronous condition occurs at the maximum of the "sine" (sinx/x) function, but this is not the only consideration when optimizing the sensitivity expression (see 3.3). Indeed this shift is visible in Fig. 11; it is worth noting that it is very small, 8% and 6% for case a) and b), respectively. These small values indicate that the method of optimization is essentially correct.

Further improvement is obtained by scaling the parameters to move the centre-band frequency up to the synchronism frequency.

Referring to curves of Fig. 11, the case a) requires 8% scaling and the case b) 6%. This means:

	a		b
s = 0.005m	→ 0.0046m	;	0.0047m
d = 0.065m	→ 0.060 m	;	0.061 m

It should be mentioned that the optimization method is an iterative one.

3.2 Optimization of the Ratio between Power in the Dielectric and Total Power

As previously outlined, power excited by the beam flows mainly between the slabs. We expect that increasing slab thickness will give a different power distribution, according to our needs.

With all other dimensions fixed an increased slab thickness changes the wave numbers p, q, γ_1, such that synchronism with the beam is lost, and this causes a transfer of the previously excited power from the air to the dielectric slabs, which tend to act like dielectric horn-antenna. This is evident from the plots of Fig. 8a); the curves refer to the case studied for the AA and are extensively described in Section 5.

Another interesting aspect of increasing the slab thickness is that we expect a change in the z-component of the electric field distribution over x. Results of computation for this change are shown in the curves of Fig. 8b). They refer to the same conditions as in Fig. 8a).

The magnitude of E_z at the air-dielectric interface decreases when the slab thickness is increased. This is an interesting result from the practical point of view since at a certain point it will be necessary to have a metallic coating on the air-dielectric interface so that the power can coupled-out of the vacuum chamber.

4. *PICK-UP DESIGN METHODS*

The considerations described in the previous section suggest that the pick-up can be designed by distinguishing between three zones:

1) the synchronous zone (where the beam excites power), length = L,

2) the optimization zone (where the ratio P_{diel}/P_{total} is increased), length = ℓ_1,

3) the transition zone from hybrid to rectangular waveguide (where each slab comes into an empty rectangular wave guide of appropriately chosen dimensions), length = ℓ_2.

A diagram of the pick-up is outlined below.

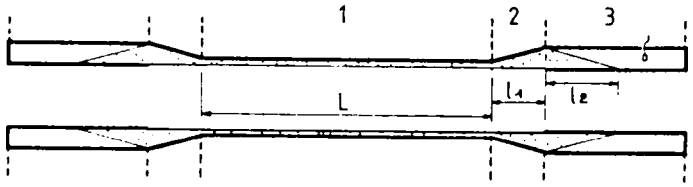

Figure 5 - Longitudinal pick-up diagram.

Moreover, the question of matching between the rectangular wave guide at zone 3 and the coaxial output cable could arise: it involves the study of the performance and matching of a pair "short antenna".

Below we list the main difficulties which can arise in each region.

Zone 1: parameters are chosen to work at a fixed frequency in synchronism with the beam. In this region only the chosen synchronous mode is above the cut-off. Problems can arise in zone 2 because computations have shown that the LSE1 mode is above the cut-off, starting from s > 9 mm. The LSM2 is also above cut-off but it can be neglected as it only starts from s > 20 mm.

The length of zone 2 is small compared to zone 1, and even if the LSE1 mode can be excited (not in synchronism) by the beam passage, it will carry very little power, as the field amplitude is proportional to the interaction length ℓ, through the factor $\ell/2 \cdot \text{sine}[k_0((1/\beta)-\bar{\gamma}_m)\ell/2]$. Moreover, the LSE fields do not interact with the principal mode of propagation, since they are orthogonal modes.

We expect that the power carried by the LSM mode is not greatly perturbed by the "smooth" change of slab sizes (see Section 5) in zone 2.

The behaviour of fields in the transition zone 3 can be estimated by performing the projection of the loaded wave guide normal modes (LSM and LSE) onto the empty rectangular wave guide modes (TE and TM).

In this particular case, the LSM1 and the LSE1 are the only incident modes on the transition section, and the TE10 mode is the only mode above the cut-off in the empty rectangular wave guide; so the computation reduces into projecting the LSM1 and LSE1 modes onto the TE10 mode.

This procedure gives an indication of the mode-matching; it furnishes an estimate for the percentage of transmitted field across the transition into the TE10 mode.

The transmitted power is computed from the transmitted field. The results of the computation lead to the choice of transition length. A high percentage of transmitted field gives us confidence that the tapered section length ℓ_2 is not too critical a point of the pick-up design, as good matching exists between the hybrid modes and the TE10 mode; on the other hand, if only a very small quantity of the incident field is transmitted into the rectangular wave guide, particular care must be devoted to the study and the design of the transition section. In our case, the computations show that half of the LSM1 power is transferred into the TE10 mode, while no projection onto the TE10 mode is possible for the LSE1 mode. Hence, we estimate a 1 to 2 λg-length for the tapered section (λg is the wave length in the empty rectangular wave guide) is sufficient to guarantee the LSM1 power transmission and decay of higher order modes excited by the LS1 mode.

It is worth noting that the transmitted power value is only an estimation, namely a lower limit, as power radiated from the tapered section is not taken into account.

The final choice of the tapered section length ℓ_2 must come from experimental tests, which can suggest the best compromise between smoothing the transition slope and minimizing the total pick-up length. Computations are reported in Appendix 2.

Metallization of the inner surface starts at zone 3, so that the beam returns to its passage inside the vacuum chamber. This point is also critical as the tangential component of electric field must die out on the metal surface. Hence, increasing the slab thickness is very useful as, at the maximum thickness, the magnitude of E_z is greatly reduced at the air-dielectric interface with respect to its value in the interaction zone. This result is evident from the curves of Fig. 8b). It is also reasonable to ensure that the metal covering does not start in a straight line along y-coordinate, but is sloped diagonally (Fig.6)

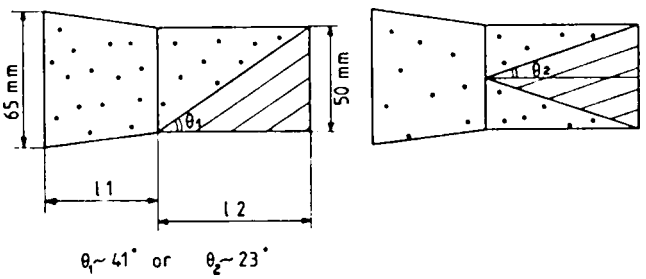

Figure 6 - Top view of pick-up ends: suggested shapes and estimation of slopes.

Such a covering presents a gradually and continuously varying discontinuity to the propagating field. Anyway, the best shape and slope must be sought experimentally.

The problem of matching the wave guide to the coaxial output line can be rather easily solved by using appropriate devices, generally supplied by specialized manufacturers. An alternative approach is to build a laboratory mock-up of this transition and then choose an antenna which introduces the least reflection in the wave guide for the best position of the shorted wave guide end face with respect to the antenna itself. Some suggestions can be found in literature[12-14]. Matching should be sought over a reasonably wide band, at least comparable with that of the pick-up.

For the AA pick-up the coaxial wave guide transition will be built in the PS Workshops. Most of the doubts concerning the end effects of the pick-up can be solved only by experimental tests in the laboratory. To this aim, work in the laboratory on an experimental mock-up started at the beginning of June. The experimental results will be published in another publication to follow.

5. *A PICK-UP FOR THE ANTIPROTON ACCUMULATOR*

The pick-up dimensions must fit the pre-existing geometry of the AA vacuum chamber (Fig. 7). Given the vacuum chamber dimensions all parameters of the pick-up can be determined as can the frequency at which beam-mode synchronism occurs. This frequency is expected to be in the neighbourhood of the maximum of the sensitivity versus frequency curve.

The fixed dimensions for the AA are:

$$b = d = 0.065 \text{ m}$$
$$s = 0.005 \text{ m}$$
$$\varepsilon_r = 3.75$$
$$\beta_p = 0.9659$$
$$L = 0.3 \text{ m}$$

The beam-mode synchronous frequency is obtained from the solution of the system of three equations (A.11b), (3.2a), (3.2b). The system is solved by computer calculation giving, for the above dimensions:

$$f_0 = 5.42 \text{ GHz} , \quad k_0 = 113.57 \text{ m}^{-1} .$$

The behaviour of the pick-up may now be investigated as a function of slab thickness.

A search for roots in the LSE dispersion equation (A.10a) and for higher order roots in LSM dispersion equation (A.11b) is first carried out as a function of slab thickness. All pick-up parameters are kept unchanged, apart from the slab thickness, which is increased up to 20 mm by steps of 1 mm each.

The system of equations (A.11b) or (A.10a) (depending on the mode under investigation), (A.9c) (A.9b) is employed: the wave numbers p, q, γ_m relating to each new value of thickness (s) are computed. The results are that LSE dispersion equation has no roots up to s = 9 mm and then no other root appears in the range of investigation up to 20 mm. The LSM dispersion equation has a second root at s = 20 mm. The propagation of these modes in the output wave guide are reported in Section 4.

As described earlier, the slab thickness is increased at the ends up to 20 mm in the hybrid wave guide, and the dielectric is inserted into the empty rectangular output wave

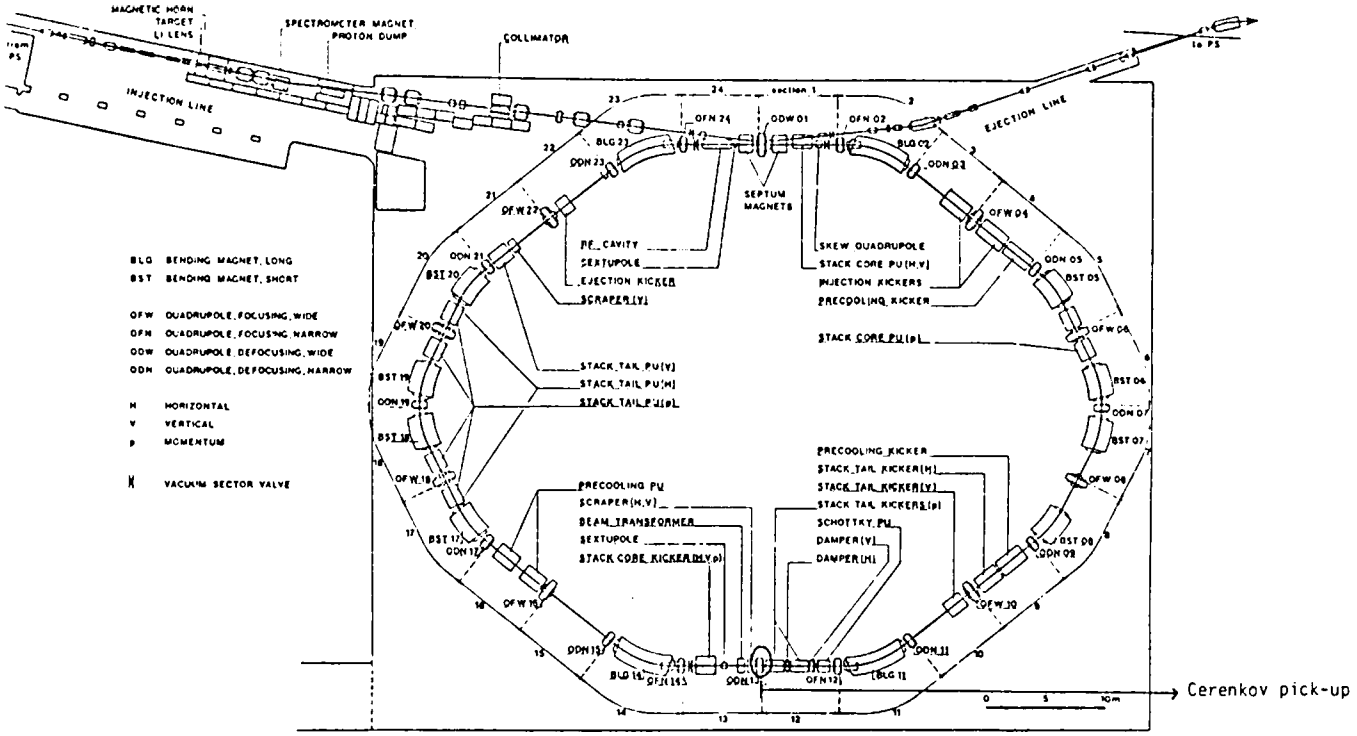

Figure 7a - Antiproton Accumulator. General layout and location of the Cerenkov pick-up.

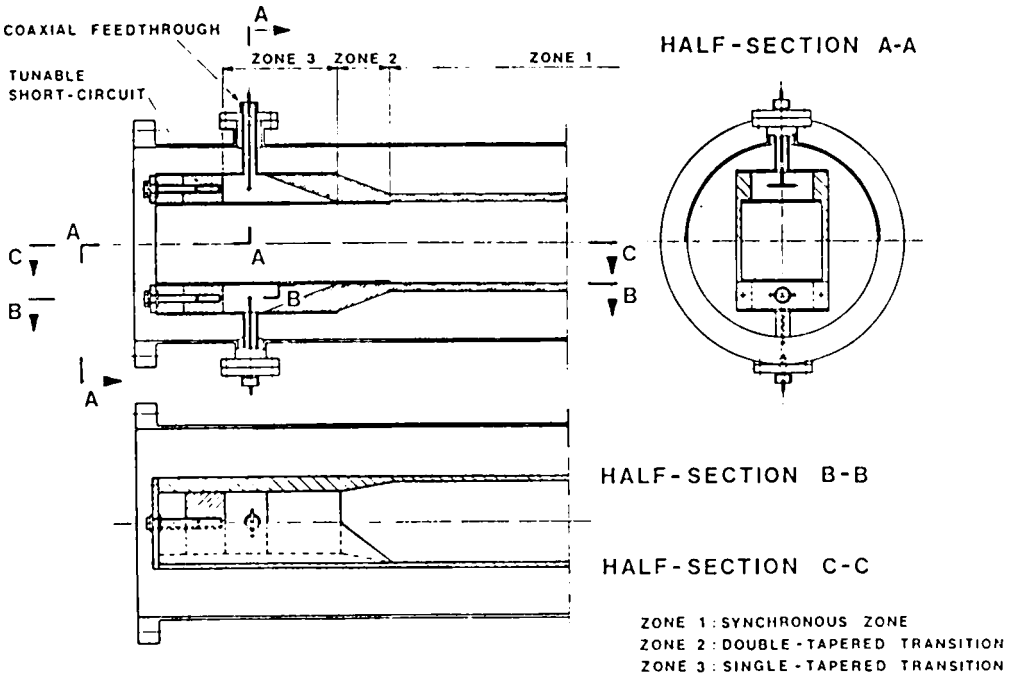

Figure 7b - Layout of the Cerenkov pick-up in the AA vacuum chamber.

guide, where again the slab thickness is smoothly decreased to zero. Referring to zone 3 of Fig. 5, two lengths are suggested for the latter transitions:

1: ℓ_2 = 75 mm, meaning slope ≈ 27% and θ = 15.3°,
2: ℓ_2 = 100 mm, meaning slope ≈ 20% and θ = 11.5°.

If the same slopes are accepted for zone 2, the overall transition becomes:

case 1: slope 27% → $\ell_1 + \ell_2$ = 131.25 mm,
case 2: slope 20% → $\ell_1 + \ell_2$ = 175 mm.

The dimensions for the empty rectangular wave guide are 50 × 20 mm; the cut-off frequency for the first mode (TE10) is about 3 GHz.

The following are the values for the cut-off frequencies of higher order modes:

TE20	6.0 GHz
TE01	~7.5 GHz
TE11, TM11	~8.1 GHz

The 50 mm width of the rectangular wave guide requires a decrease in slab width, occurring over the length during which the thickness increases. An even smaller width would be better from the point of view of increasing further the cut-off frequency of TE20 mode. The 50 mm choice is a compromise to simplify manufacture.

The density distribution of power propagating along $\hat{z}$ (P_z) versus x and the distribution of the z-component of the electric field (E_z) versus x is calculable from the theory for increasing slab thickness. Figure 8a) shows plots of the function

$$\frac{1}{P_{TOT}} \cdot \frac{dP_z}{dx} \tag{5.1}$$

versus x. From this expression, it is obvious that the dimensions of the ordinate axis in Fig. 8a) is [length]$^{-1}$ while, for convenience, lengths on the abscissae axis are expressed in terms of the normalized variable $xk_0 = 2x\pi/\lambda_0 = \bar{x}$. Figure 8b) contains plots of the z-component of the electric field, valid at y = b/2 (and normalized by an "excitation" factor) versus $\bar{x}$. Dimensions of ordinate axis are Volt/m; the magnitude must be multiplied by the excitation factor, which is defined as follows:

$$\frac{\cos \bar{p}\bar{s}}{\sinh \bar{q}\bar{d}/2} \cdot \frac{\bar{k}_p \bar{q} \varepsilon_r \sqrt{Z_0}\, k_0 I_0 L/2}{[(1+\bar{q}^2)\bar{k}_p \bar{b} \varepsilon_r \bar{G}_o]^{1/2}} \approx 110\, I_0 L/2 \quad . \tag{5.2}$$

In all of the above all parameters refer to the synchronous LSM1 mode; other symbols have already been previously defined. The zero of abscissae axis is assumed at the centre of the wave guide total width. The half distance between slabs corresponds to $\bar{x}$ = 3.69. For case 1 in Figs 8a) and 8b) the synchronous condition is satisfied and $\bar{s}$ = 0.57 (in reality s = 0.005 m).

The power and E_z distribution shown in the above figures confirm that good coupling with the beam requires a strong electromagnetic field in the air zone. Indeed for case 1 it is evident that most of the power is to be found between the slabs: the ratio between

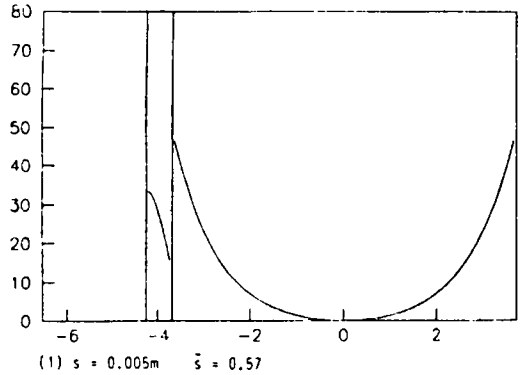

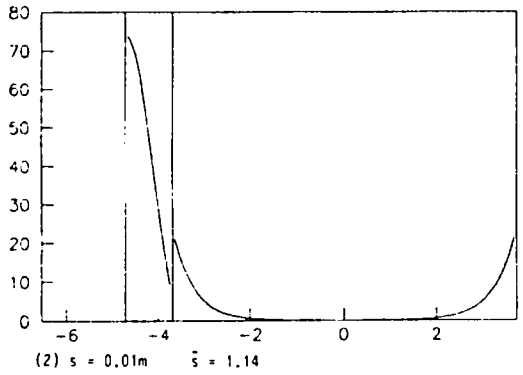

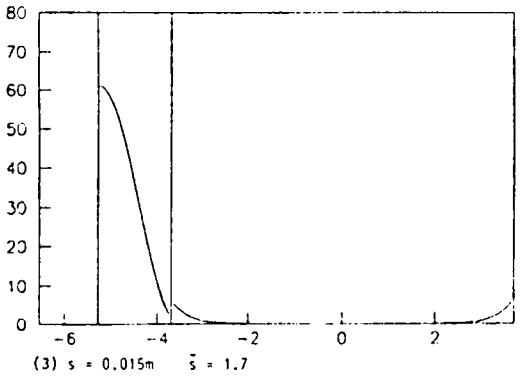

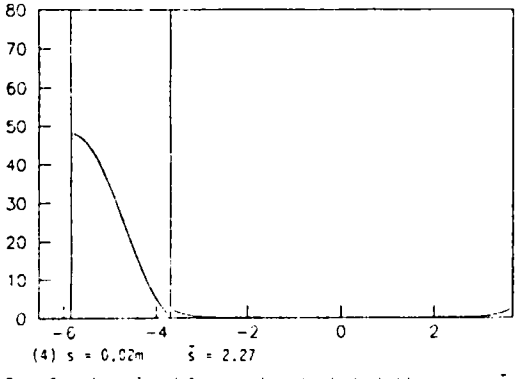

Fig. 8a - Normalized z-power density distribution versus $\bar{x}$ ($= 2\pi x/\lambda_c$) at different slab thicknesses.

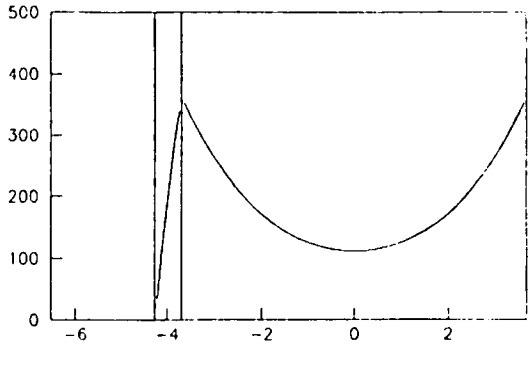

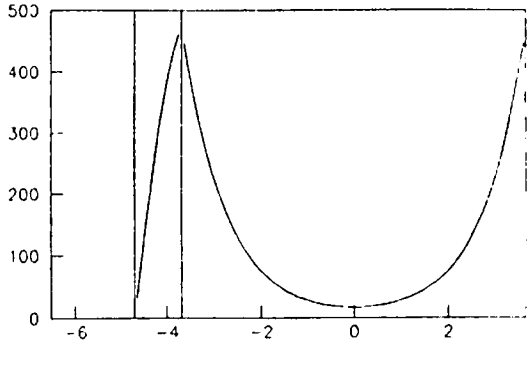

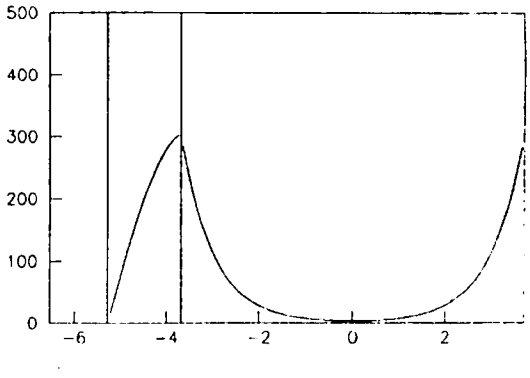

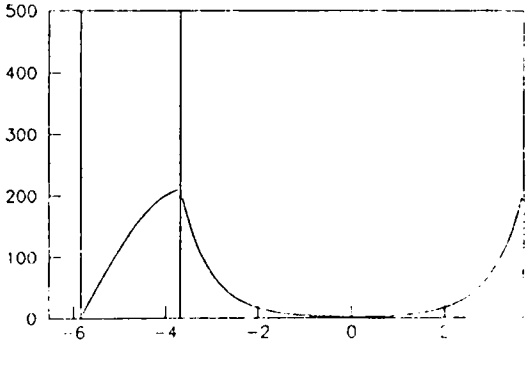

Fig. 8b - Normalized electric field z-component at y = b/2 versus $\bar{x}$, at different slab thicknesses.

and total power is 0.26. Case 2 refers to $\bar{s}$ = 1.14 (s = 0.01 m). This shows an already significant change in power distribution: power ratio value is now 0.87.

As q increases with slab thickness, the dependence of E_z on x becomes more rapid (see A.18c): it decreases its amplitude almost everywhere, except for the neighbouhood of air-dielectric interface. Increasing the slab thickness even further decreases E_z at the dielectric-air interface as can be seen from case 3 and 4. The latter refer respectively to:

3: $\bar{s}$ = 1.7 (s = 0.015 m) 4: $\bar{s}$ = 2.27 (s = 0.02 m) .

These last two curves yield a very convenient shape for the power density distribution; the power ratio values are respectively c) = 0.97 and d) = 0.99.

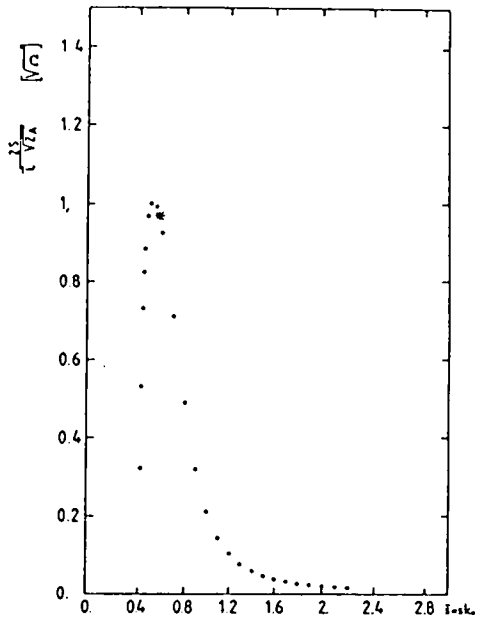

Figure 9

The AA pick-up Sensitivity at sychronism versus normalized slab thickness.

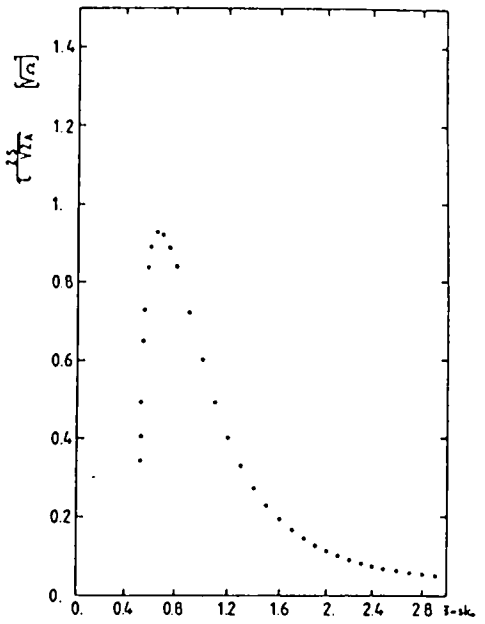

Figure 10

Sensitivity at synchronism versus normalized slab thickness: the same cross section dimensions as the AA pick-up, but ε_r = 2.55.

For the ε_r and the distance between slabs chosen for the AA pick-up, the sensitivity versus normalized slab thickness is given in Fig. 9. The procedure used to obtain this figure is described in Section 3.

The function on the ordinate axis of Fig. 9 is the sensitivity in units of equivalent length of the slab $\bar{L}$, divided by the constant factor $\sqrt{Z_A}$: in other words the function plotted is the expression (3.4) divided by $\bar{L}/2 = Lk_0/2 = L\pi/\lambda_0$ and by $\sqrt{Z_A}$.

Values of $\bar{s} = sk_0$, the equivalent slab thickness, are plotted on the abscissae of Fig. 9. Hence, due to the factor $\sqrt{Z_A}$, the dimensions of sensitivity in Fig. 9 become ohms (Ω).

The same function is plotted in Fig. 10, but for a different value of ε_r.

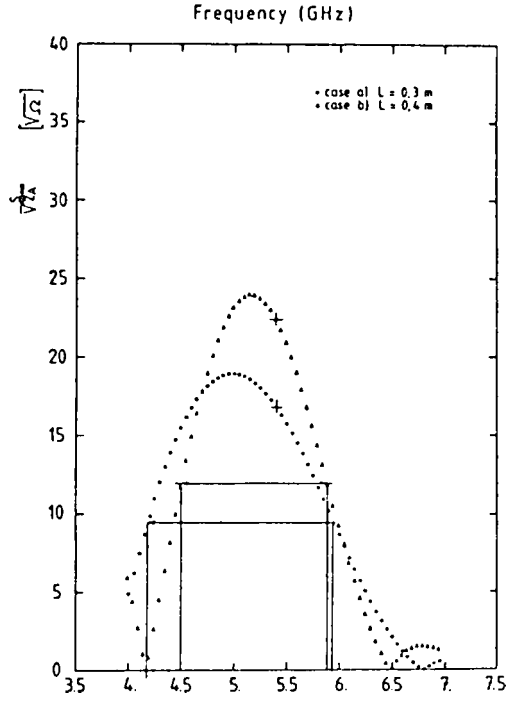

Figure 11

The AA pick-up Sensitivity for the LSM1 mode versus frequency. Arrows indicate the 3 dB bandwidth: it is about 1.8 and 1.4 GHz for case a) and b) respectively. The cross indicates the frequency for beam-mode synchronism.

Since $\bar{q}$ decreases with $\bar{s}$, both figures show a minimum $\bar{s}$, depending on the fixed β_p ; it is determined by the requirement of a real value of the k_y wave number (= π/b) in equation (3.2b). It can be seen that the $\bar{s}$ value corresponding to the maximum of sensitivity increases with ε_r decreasing. The star point on Fig. 9 is placed at $\bar{s}$ = 0.57; this is the working point of the design for the AA pick-up; it is not too far from the optimum.

A maximum possible value of $\bar{s}$ also exists: it comes from the upper limit for $\bar{q}$ ($\bar{q}$ = 1.658 or 1.245 for ε_r = 3.75 or 2.55, respectively), since $\bar{q}$ must always give a real $\bar{p}$ in (A.9c).

The graph of Fig. 11 is again sensitivity divided by the factor $\sqrt{2_A}$, but this time (from expression (3.3)) versus frequency.

The two curves refer to the AA pick-up design, but they differ in the length of the "synchronous zone", which is respectively 0.3 m for the case a) and 0.4 m for the case b). Both curves show a cut-off frequency at about 4 GHz, below which the LSM dispersion relation has no root. The main differences between the two curves in Fig. 11 arise from sine$[k_0((1/\beta_p) - \bar{\gamma}_m)L/2]$ term; the maximum amplitude decreases for a smaller length because of the L/2 factor appearing in the expression for the sensitivity (3.3).

For the smaller L value, the sensitivity curve is broadened and the frequency of maximum response of the pick-up is shifted towards lower values.

Hence, bandwidth is inversely proportional to slab length: in the two cases described, estimated bandwidth values are respectively: a) ~1.8 GHz and b) ~1.4 GHz.

The frequency for beam-mode synchronism is indicated by a cross on each curve of Fig. 11: it does not correspond to the value for the maximum response of the pick-up. Following the method outlined in Section 3, scaling the cross-section dimensions of the pick-up can shift the maximum of the response nearer to the beam-mode synchronism frequency.

In conclusion, the energy lost by one charged particle passing once through the design adopted for the AA pick-up is:

case a) L = 0.3 m $\quad \Delta E = 2.2 \cdot 10^{-17}$ eV

case b) L = 0.4 m $\quad \Delta E = 3.9 \cdot 10^{-17}$ eV

This energy is spread throughout the bandwidth of around 1.4 to 1.8 GHz depending upon the length chosen. Figure 7 gives the dimensions and layout of the pick-up designed for measurements in the AA. The revolution frequency of a particle in the AA is 1.855 MHz so that the power generated in the pick-up may be calculated.

ACKNOWLEDGEMENTS

I want to thank heartily E. Jones for his continuous support, Steve Hancock for his friendly help and Profs G. Di Massa and V. Vaccaro for the fruitful discussions and comments.

REFERENCES

1. E. Brambilla, G. Di Massa, E. Jones and V.G. Vaccaro, Pick-ups for very High Frequencies, In preparation.

2. J. Jelley, Cerenkov radiation and its Applications, London: Pergamon, 1958.

3. B.M. Bolotowski, Theory of Cerenkov Radiation (III), Soviet Physics Uspekhi, Vol. 4, No 5, March-April 1962.

4. V.P. Zrelov, Cerenkov Radiation in High-Energy Physics, Atomizdat, Moskva 1968. Translated from Russian 1970.

5. M. Abele, L'Effet Cerenkov en Optique et dans le Domaine des Micro-Ondes, Nuovo Cimento, Supplemento al Vol. 9, 1952.

6. H. Lashinsky, Generation of Microwaves by Cerenkov Radiation, Proceedings of the Symposium on Millimeter Waves, New York 1959.

7. Paul D. Coleman and C. Enderby, Megavolt Electronics Cerenkov Coupler for the Production of Millimeter and Submillimeter Waves, Journal of Applied Physics, Vol. 31, 1960.

8. J.E. Walsh, T.C. Marshall, M.R. Ross and S.P. Schlesinger, Relativistic Electron-Beam-Generated Coherent Submillimeter Wavelength Cerenkov Radiation, IEEE Trans. on MTT, Vol. MTT 25, No. 6, June 1977.

9. R.E. Collin, Field Theory of Guided Waves, McGraw-Hill Book Company, New York, 1960.

10. J. Van Bladel, Electromagnetic Fields, McGraw-Hill Book Company, New York, 1964.

11. F.E. Gardiol, Higher Order Modes in Dielectrically Loaded Rectangular Waveguides, IEEE Trans. on MTT, Vol. MTT-16, No. 11, Nov. 1968.

12. R.E. Collin, Fundations of Microwave Engineering, McGraw-Hill Book Company, New York, 1966, pp 183-190.

13. S. Ramo, J.R. Whinnery and T. Van Duzer, Fields and Waves in Communication Electronics, 2nd Edition, Wiley, 1965, pp. 431-433.

14. T. Moreno, Microwave Transmission Design Data, McGraw-Hill Book Company, New York, 1948, pp. 176-178.

APPENDIX 1

COMPUTATION OF THE NORMAL MODES FOR A DIELECTRIC SLAB-LOADED WAVE GUIDE

For the sake of completeness the method for computing the normal modes of a loaded wave guide and the related expressions used in previous sections are given below. Rectangular loaded wave guides have been exhaustively studied both in text-books[9,10] and papers[11].

The normal modes propagating in such kinds of wave guides are hybrid modes, with both $\vec{E}$ and $\vec{H}$ components along the axis of the wave guide.

Following Collin we choose to classify the normal modes of the wave guide under examination (Fig. 1) as either LSE (longitudinal section electric) or LSM (longitudinal section magnetic).

Fields can be derived from the hertzian type potentials: the electric one $\vec{\Pi}^{el}$ for LSM modes, and the magnetic one $\vec{\Pi}^{h}$ for LSE modes, through the following equations:

LSE modes

$$\vec{e} = -j\omega\mu_0 \nabla \cdot \vec{\Pi}^{h} \qquad (A.1a)$$

$$\vec{h} = \nabla \cdot \nabla \cdot \vec{\Pi}^{h} \qquad (A.1b)$$

LSM modes

$$\vec{e} = \nabla \cdot \nabla \cdot \vec{\Pi}^{el} \qquad (A.2a)$$

$$\vec{h} = j\omega\varepsilon_0\varepsilon_r(x) \nabla \cdot \vec{\Pi}^{el} \qquad (A.2b)$$

Hertzian potentials must satisfy the equation:

$$\nabla^2\vec{\Pi}^{el,h} + \varepsilon_r(x)k_0^2\vec{\Pi}^{el,h} = 0 \ , \qquad (A.3)$$

where $k_0^2 = \omega^2\varepsilon_0\mu_0$ is the propagation constant of unbounded empty space.

The equations (A.1), (A.2) and (A.3) are valid in each region where $\varepsilon_r(x)$ is constant

Referring to the structure of Fig. 1, the solution of (A.3) is a hertzian potential with only an x-component, for both LSE and LSM modes:

$$\vec{\Pi}^{el,h} = p^{el,h}(x,y)e^{-j\gamma_m z} e^{j\omega t} \hat{x} \ . \qquad (A.4)$$

In (A.4) the propagation along z has been assumed according to $e^{-j\gamma_m z}$, where γ_m refers to the propagation constant of a generic mode. In the empty region of the wave guide the general solution is a superimposition of an even and an odd solution with respect to $x = a/2$.

The expressions for the solution of (A.3) are given as:

LSE modes

$$p^{h}_{e,o}(x,y) = \left\{ \begin{array}{l} E_e \sin px \\ E_o \sin px \\ \\ F_e \cosh q(x - a/2) \\ F_o \sinh q(x - a/2) \\ \\ E_e \sin p(a - x) \\ -E_o \sin p(a - x) \end{array} \right\} \cos\left(\frac{n\pi}{b}\, y\right) \qquad (A.5)$$

$$F_e = E_e \frac{\sin ps}{\cosh qd/2} \qquad (A.6a) \qquad F_o = - E_o \frac{\sin ps}{\sinh qd/2} \qquad (A.6b)$$

LSM modes

$$p^{el}_{e,o}(x,y) = \left\{ \begin{array}{l} A_e \cos px \\ A_o \cos px \\ \\ B_o \sinh q(x - a/2) \\ B_e \cosh q(x - a/2) \\ \\ A_e \cos p(a - x) \\ -A_o \cos p(a - x) \end{array} \right\} \sin\left(\frac{n\pi}{b}\, y\right) \qquad (A.7)$$

$$B_e = A_e\, \varepsilon r \frac{\cos ps}{\cosh qd/2} \qquad (A.8a) \qquad B_o = - A_o\, \varepsilon r \frac{\cos ps}{\sinh qd/2} \qquad (A.8b)$$

where e,o subscripts indicate even or odd solutions.

In the above expressions, the k_x wave number (in the air- or vacuum-region) is assumed to be imaginary, in accord with section 1; hence,

$$p^2 = \varepsilon_r\, k_0^2 - (n\pi/b)^2 - \gamma_m^2 \qquad (A.9a)$$

$$q^2 = - k_0^2 + (n\pi/b)^2 + \gamma_m^2 \qquad (A.9b)$$

where $ik_x(air) = q$, $k_x(diel) = p$, $k_y = n\pi/b$.

It is useful to replace (A.9) by

$$p^2 + q^2 = (\varepsilon_r - 1)k_0^2 \quad . \qquad (A.9c)$$

Imposing the continuity conditions at the air-dielectric interface, the following trascendental equations are obtained:

LSE modes

$$\text{even } \pi^h \qquad p \operatorname{cotg} ps = -q \tanh qd/2 \qquad (A.10a)$$

$$\text{odd } \pi^h \qquad p \operatorname{cotg} ps = -q \coth qd/2 \qquad (A.10b)$$

LSM modes

$$\text{even } \Pi^{el} \qquad p \operatorname{tg} ps = \varepsilon_r q \operatorname{tgh} qd/2 \tag{A.11a}$$

$$\text{odd } \Pi^{el} \qquad p \operatorname{tg} ps = \varepsilon_r q \operatorname{cotgh} qd/2 \ . \tag{A.11b}$$

Equations (A.10) and (A.11) will be referred to as "dispersion equations".

Each of the dispersion equations together with (A.9c) determines an infinite number of solutions for the wave numbers p and q. So each mode will be marked by two subscripts m, n: the first referring to the order of the wave number along the x-coordinate, the other to the order of the wave number along y.

The following orthogonality relation holds for the transverse components of fields belonging to different modes:

$$\iint_S (\underline{e}_{mn} \cdot \underline{h}^*_{ik}) \cdot \hat{z} \, da = 0 \ , \qquad \text{if } m \neq i \text{ and } n \neq k \tag{A.13}$$

where S is the wave guide cross-sectional area and $\hat{z}$ is the vector along the axis of the wave guide.

Imposing normalization of eigenvectors by (A.13), we can determine the unknown factors of (A.5) and (A.7).

LSM modes

$$A_{e,o} = \{[k_0^2 + q^2]\omega\varepsilon_0\varepsilon_r\gamma_m \, b \, G_{e,o}\}^{-1/2} \tag{A.14}$$

with

$$G_e = \frac{1}{2}\left[s\left(1 + \frac{\sin 2ps}{2ps}\right) + \varepsilon_r \frac{d}{2} \frac{\cos^2 ps}{\cosh^2 qd/2} \cdot \left(1 + \frac{\sinh qd}{qd}\right)\right] \tag{A.15a}$$

$$G_0 = \frac{1}{2}\left[s\left(1 + \frac{\sin 2ps}{2ps}\right) + \varepsilon_r \frac{d}{2} \frac{\cos^2 ps}{\sinh^2 qd/2} \cdot \left(\frac{\sinh qd}{qd} - 1\right)\right] \tag{A.15b}$$

LSE modes

$$E_{e,o} = \{[k_0^2 + q^2]\omega\mu_0\gamma_m \, b \, L_{e,o}\}^{-1/2} \tag{A.16}$$

with

$$L_e = \frac{1}{2}\left[s\left(1 - \frac{\sin 2ps}{2ps}\right) + \frac{d}{2} \frac{\sin^2 ps}{\cosh^2 qd/2} \cdot \left(1 + \frac{\sinh qd}{qd}\right)\right] \tag{A.17a}$$

$$L_0 = \frac{1}{2}\left[s\left(1 - \frac{\sin 2ps}{2ps}\right) + \frac{d}{2} \frac{\sin^2 ps}{\sinh^2 qd/2} \cdot \left(\frac{\sinh qd}{qd} - 1\right)\right] \tag{A.17b}$$

For convenience we list below the relative expressions both for LSM and LSE modes:

LSM modes

$$e_x(x, y) = (k_0^2 + q^2) P_o^{el}(x, y) \tag{A.18a}$$

$$e_y(x, y) = \frac{\partial}{\partial y} \frac{\partial}{\partial x} P_o^{el}(x, y) \tag{A.18b}$$

$$e_z(x, y) = -j\gamma_m \frac{\partial}{\partial x} P_o^{el}(x, y) \tag{A.18c}$$

$$h_x(x, y) = 0 \tag{A.19a}$$

$$h_y(x, y) = \omega\gamma_m \varepsilon_0\varepsilon_r(x) P_o^{el}(x, y) \tag{A.19b}$$

$$h_z(x, y) = -j\omega \varepsilon_0\varepsilon_r(x) \frac{\partial}{\partial y} P_o^{el}(x, y) \tag{A.19c}$$

LSE modes

$$e_x(x, y) = 0 \tag{A.20a}$$

$$e_y(x, y) = -\omega\mu_0 \gamma_m P_e^h(x, y) \tag{A.20b}$$

$$e_z(x, y) = j\omega\mu_0 \frac{\partial}{\partial y} P_e^h(x, y) \tag{A.20c}$$

$$h_x(x, y) = (k_0^2 + q^2) P_e^h(x, y) \tag{A.21a}$$

$$h_y(x, y) = \frac{\partial}{\partial y} \frac{\partial}{\partial x} P_e^h(x, y) \tag{A.21b}$$

$$h_z(x, y) = -j\gamma_m \frac{\partial}{\partial x} P_e^h(x, y) \tag{A.21c}$$

APPENDIX 2

PROJECTION OF THE HYBRID MODES ON THE EMPTY RECTANGULAR WAVE GUIDE NORMAL MODES

1. OUTLINE OF THE METHOD

The incident field is written as an expansion of the normal modes of the empty rectangular wave guide. From previous theory, the incident field is a sum of the principal beam-excited mode (LSM1) and the higher order mode (LSE1), which arises in zone 2 (see Section 4). Hence,

$$\underline{E}_b(\text{LSM1}) + \underline{E}_b(\text{LSE1}) = \sum_{mn} a_{mn}\, \underline{\tilde{e}}_{mn} \quad . \tag{A.22}$$

where $\underline{\tilde{e}}_{mn}$ represents the generic normal mode function in the empty rectangular wave guide and E_b is the beam excited field.

If we now take into account that only the TE10 mode is above cut-off in the rectangular wave guide, (A.22) reduces:

$$\underline{E}_b(\text{LSM1}) + \underline{E}_b(\text{LSE1}) = a_{10}\, \underline{\tilde{e}}_{10} \quad . \tag{A.23}$$

It holds (see Section 2) that:

$$\underline{E}_b(\text{LSM1}) = F\, \underline{e}_1(\text{LSM}) \tag{A.24a}$$

$$\underline{E}_b(\text{LSE1}) = F'\underline{e}_1(\text{LSE}) \tag{A.24b}$$

where $\underline{e}_1$ (LSM or LSE) refers to the normal mode eigenvector in the hybrid wave guide, and F and F' are the mode excitation factors from the beam.

Remember that the wave numbers related to mode functions $\underline{e}_1$ depend on the maximum slab thickness, $s = 20$ mm, where the transition starts. The following orthogonality property holds for the rectangular wave guide mode functions:

$$\iint_S (\underline{\tilde{e}}_{mn} \times \underline{\tilde{h}}^*_{ij}) \cdot \hat{z}\, da = 0 \quad \text{if } m \neq i \text{ or } n \neq j \tag{A.25}$$

where S is the wave guide cross-section and da is an indifinitesimal surface element.

Hence, we can perform a cross product with $(\underline{\tilde{h}}_{10})^*$ on both sides of (A.23) and, employing (A.25), we can evaluate the coefficient a_{10}.

2. FIELD EXPRESSIONS

We are interested into the hybrid mode configurations in the dielectric region. In order to use the standard notation for the normal modes of rectangular wave guides, we write the hybrid mode fields (A.18 ÷ A.21) in a coordinate frame with the x-axis along the long side (b) of the dielectric slab and the y-axis along the short one (s) (Fig. 12). The complete set of expressions is given below:

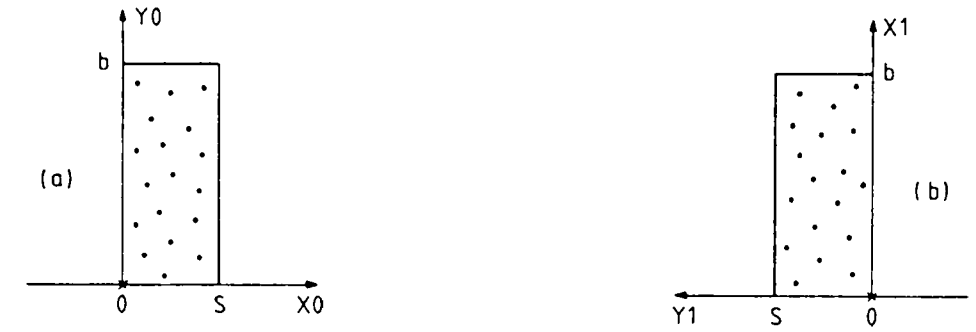

a) Previously used hybrid wave guide frame *b) Usual rectangular wave guides frame*

Figure 12

LSM1 mode

$$e_{x_1} = -\frac{\pi}{b} p_m [A_0]_m \sin[p_m(s - y_1)] \cos\left(\frac{\pi}{b} x_1\right) \quad \text{(A.26a)}$$

$$e_{y_1} = -(k_0^2 + q_m^2)[A_0]_m \cos[p_m(s - y_1)] \sin\left(\frac{\pi}{b} x_1\right) \quad \text{(A.26b)}$$

$$e_{z_1} = j \gamma_m p_m [A_0]_m \sin[p_m(s - y_1)] \sin\left(\frac{\pi}{b} x_1\right) \quad \text{(A.26c)}$$

$$h_{x_1} = \omega \epsilon_0 \epsilon_r \gamma_m [A_0]_m \cos[p_m(s - y_1)] \sin\left(\frac{\pi}{b} x_1\right) \quad \text{(A.26d)}$$

$$h_{y_1} = 0 \quad \text{(A.26e)}$$

$$h_{z_1} = -j \omega \epsilon_0 \epsilon_r \frac{\pi}{b} [A_0]_m \cos[p_m(s - y_1)] \cos\left(\frac{\pi}{b} x_1\right) \quad \text{(A.26f)}$$

LSE1 mode

$$e_{x_1} = -\omega \mu_0 [E_e]_m \gamma_m \sin[p_m(s - y_1)] \cos\left(\frac{\pi}{b} x_1\right) \quad \text{(A.27a)}$$

$$e_{y_1} = 0 \quad \text{(A.27b)}$$

$$e_{z_1} = -j\omega\mu_0 \frac{\pi}{b} [E_e]_m \sin[p_m(s - y_1)] \sin\left(\frac{\pi}{b} x_1\right) \quad \text{(A.27c)}$$

$$h_{x_1} = - p_m \frac{\pi}{b} [E_e]_m \cos[p_m(s - y_1)] \sin\left(\frac{\pi}{b} x_1\right) \qquad (A.27d)$$

$$h_{y_1} = - (k_0^2 + q_m^2)[E_e]_m \sin[p_m(s - y_1)] \cos\left(\frac{\pi}{b} x_1\right) \qquad (A.27e)$$

$$h_{z_1} = - j \gamma_m p_m [E_e]_m \cos[p_m(s - y_1)] \cos\left(\frac{\pi}{b} x_1\right) \qquad (A.27f)$$

TE10 mode

$$e_{x_1} = 0 \qquad (A.28a)$$

$$e_{y_1} = \sin\left(\frac{\pi}{b} x_1\right) \qquad (A.28b)$$

$$e_{z_1} = 0 \qquad (A.28c)$$

$$h_{x_1} = - \frac{1}{Z_{TE}} \sin\left(\frac{\pi}{b} x_1\right) \qquad (A.28d)$$

$$h_{y_1} = 0 \qquad (A.28e)$$

$$h_{z_1} = j \frac{1}{\eta} \frac{\lambda}{2b} \cos\left(\frac{\pi}{b} x_1\right) \qquad (A.28f)$$

The amplitude of the TE10 mode is determined by the coefficient a_{10}. The subscript "1" below the x and y coordinates indicates that the above expressions (A.26 ÷ A.28) are written in the rectangular wave guide frame: they hold for $x_1 \in [0, b]$, $y_1 \in [0, s]$. The subscript "m" in (A.26), (A.27) for p, q, A_0 and E_e indicates that these values depend on slab thichness. A_0 and E_e refer to expressions (A.14) and (A.16) of Appendix 1.

In (A.28),

η = the intrinsic impedence of the medium filling the wave guide; for the vacuum, $\eta = \sqrt{\mu_0/\varepsilon_0} = Z_0$,

$Z_{TE} = Z_0[1 - (f_c/f)^2]^{-1/2}$

with

$f_c = 1/2b\sqrt{\varepsilon\mu}$,

ε, μ = the absolute dielectric constant and permeability of medium filling the wave guide (in this case the vacuum: ε_0, μ_0),

f = the working frequency,

λ = the wavelength in the unbounded medium: for vacuum $\lambda = \lambda_0 = c/f$.

3. *EVALUATION OF THE COEFFICIENT A_{10}*

The computations described at the beginning of this Appendix can now be executed. From (A.23)

$$F \iint_S \left[\underline{e}_1(\mathrm{LSM}) \cdot (\tilde{\underline{h}}_{10})^* \right] \cdot \hat{z}\, da + F' \iint_S \left[\underline{e}_1(\mathrm{LSE}) \cdot (\tilde{\underline{h}}_{10})^* \right] \cdot \hat{z}\, da = \frac{a_{10}\, sb}{2 z_{TE}} \qquad (A.29)$$

The integrals appearing on left-hand side of (A.29) are evaluated separately below.

$$\iint_S \left[\underline{e}_1(\mathrm{LSE}) \cdot (\tilde{\underline{h}}_{10})^* \right] \cdot \hat{z}\, da \ . \qquad (A.30)$$

The z-component of the cross product in (A.30) is zero, as it is $\tilde{h}_{y_{10}} = 0$ or $e_{y_1}(\mathrm{LSE}) = 0$, alternatively.

A complete mismatching occurs between the TE10 and LSE modes; hence, the latter excites only higher order modes.

$$\iint_S [\underline{e}_1(\mathrm{LSM}) \cdot (\tilde{\underline{h}}_{10})^*] \cdot \hat{z}\, da = - (k_0^2 + q_m^2)(A_o)_m \frac{1}{z_{TE}} \frac{\sin p_m s}{p_m} \cdot \frac{b}{2} \ . \qquad (A.31)$$

Hence, from (A.29):

$$a_{10} = - F(k_0^2 + q_m^2)(A_o)_m \frac{\sin p_m s}{p_m s} \ , \qquad (A.32)$$

and the transmitted field can be written:

$$\underline{E}_T = a_{10}\, \tilde{\underline{e}}_{10}$$

$$\underline{H}_T \cdot \hat{z} = \underline{E}_T / z_{TE} \qquad (A.33b)$$

4. *TRANSMITTED POWER*

Expressions (A.33) let us compute the transmitted power:

$$P_z^{\psi}(T) = \frac{1}{2} \mathrm{Re} \int_0^b dx_1 \int_0^s dy_1\, (\underline{E}_T \cdot \underline{H}_T^*) \cdot \hat{z} = \frac{1}{2} \frac{|F|^2}{z_{TE}} \left[(k_0^2 + q_m^2)(A_o)_m \frac{\sin p_m s}{p_m s} \right]^2 \frac{sb}{2} \qquad (A.34)$$

where F (the LSM1 mode excitation factor) is:

$$F = j\, k_p\, q\, \varepsilon_r [A_o] \frac{\cos ps}{\sinh qd/2} I_0 \frac{L}{2} \ . \qquad (A.35)$$

all the quantities are evaluated for the synchronous mode.

In (A.34) we recognize that

$$\frac{1}{2}\,|F|^2 = P_z^{\Psi}(\mathrm{LSM1}) \ ,$$

with $P_z^{\Psi}(\mathrm{LSM1})$ the total power the beam excites in the LSM1 mode, while other terms in (A.34) give the power transmission factor T, written below in terms of non-dimensional (normalized) quantities, for computation convenience:

$$T = \frac{Z_0}{Z_{TE}} \ \frac{(1 + \bar{q}_m^2)}{\bar{\gamma}_m \ \epsilon_r [\bar{G}_0]_m} \left(\frac{\sin \bar{p}_m \bar{s}}{\bar{p}_m \bar{s}} \right)^2 \frac{\bar{s}}{2} \quad . \tag{A.36}$$

Numerical valuation of (A.36) gives:

$$T = 0.265 \ . \tag{A.37}$$

Remembering that the previous analysis refers to one slab only, (A.37) must be multiplied by 2. Hence, we estimate that the power collected from both slabs is at least

$$0.53 \ P_z^{\Psi}(\mathrm{LSM1}) \quad .$$

APPENDIX 3

PROOF OF EQUALITY (2.9)

Stoke's theorem is applied to the vector $I_{ez}\underline{h}_m^*$: this is the product of a scalar function, the longitudinal component of current, and a vectorial one, the complex conjugate of the hybrid mode eigenvector $\underline{h}_m$.

$$\oint_C [I_{ez}(\underline{t})\underline{h}_m^*(\underline{t})] \cdot d\vec{\ell} = \iint_S i_n \cdot [\nabla \cdot I_{ez}(\underline{t})\underline{h}_m^*(\underline{t})]da \qquad (A.38)$$

where C is the boundary of the surface S, $d\ell$ is an infinitesimal step on the integration path, oriented so that the vector i_n is normal to the surface, and da is an infinitesimal surface element. The vector $\underline{t}$ is inserted to indicate the transverse dependence of the quantities: from here onwards, however, it will be dropped. In our case, S is the cross-section of the loaded wave guide and $i_n \equiv \hat{z}$.

Since

$$\nabla \cdot (I_z\underline{h}_m^*) = \nabla I_z \cdot \underline{h}_m^* + I_z \nabla \cdot \underline{h}_m^*$$

we can write (A.38) as:

$$\oint_C (I_z\underline{h}_m^*) \cdot d\vec{\ell} = \iint_S \hat{z} \cdot (\nabla I_z \cdot \underline{h}_m^*)da + \iint_S \hat{z} \cdot (I_z \nabla \cdot \underline{h}_m^*)da \quad . \qquad (A.39)$$

The z-component of a curl is involved on the right of (A.39), so no change is caused in the previous expression if the operator ∇ is replaced by its transverse component, $\nabla_t = i_x(\partial/\partial x) + i_y(\partial/\partial y)$. Hence,

$$\oint_C (I_z\underline{h}_m^*) \cdot d\vec{\ell} = \iint_S \hat{z} \cdot (\nabla_t I_z \cdot \underline{h}_m^*)da + \iint_S \hat{z} \cdot I_z(\nabla_t \cdot \underline{h}_m^*)da \quad . \qquad (A.40)$$

The term on the left of (A.40) is zero, since $I_z = 0$ on the boundary C of the wave guide (see expr. 2.1 for the current).

Thus,

$$\iint_S \hat{z} \cdot (\nabla_t I_z \cdot \underline{h}_m^*)da = - \iint_S \hat{z} \cdot I_z(\nabla_t \cdot \underline{h}_m^*)da \quad . \qquad (A.41)$$

Let us consider the equation for $\underline{h}_m^*$ coming from Maxwell's equations projected onto the axis of the wave guide:

$$\nabla_t \cdot (\underline{h}_m^* \times \hat{z}) = -j\omega\varepsilon(x)\, e_{zm}^* \quad . \tag{A.42}$$

As before, $\varepsilon(x)$ depends on the wave guide region where (A.42) is written.

Now

$$\nabla_t \cdot (\underline{h}_m^* \times \hat{z}) = \hat{z} \cdot (\nabla_t \times \underline{h}_m^*) - h_m^* \cdot (\nabla_t \times \hat{z})$$

and

$$\nabla_t \times \hat{z} = 0$$

as $\hat{z}$ is a constant vector .

We can write (A.42) as:

$$\hat{z} \cdot (\nabla_t \times \underline{h}_m^*) = -j\omega\varepsilon(x)\, e_{z_m}^* \quad .$$

Hence,

$$\iint_S \hat{z} \cdot (\nabla_t I_z \times \underline{h}_m^*)\, da = j\omega\varepsilon(x) \iint_S I_z\, e_{z_m}^*\, da \quad . \tag{A.43}$$